PHYSICAL REVIEW C

NUCLEAR PHYSICS

THIRD SERIES, VOLUME 35, NUMBER 1 JANUARY 1987

Phenomenological wave functions for the ground and 2.313 MeV states in ^{14}N

R. L. Huffman,* J. Dubach, R. S. Hicks, and M. A. Plum†

Department of Physics and Astronomy, University of Massachusetts, Amherst, Massachusetts 01003

(Received 3 September 1986)

Transverse electron scattering form factors have been measured for elastic scattering and for the transition to the 2.313 MeV state in ^{14}N. Existing structure models could not simultaneously describe the two $M1$ form factors. Consequently, new phenomenological wave functions were determined by fitting the electron scattering results and other observables. For the 2.313 MeV transition, the new wave functions give smaller $L=2$ transition amplitudes than the earlier models. This reduction and the deduced value for the $L=0$ transition amplitude appear to be supported by the measurements of the ^{14}N(p,p')^{14}N, ^{14}C(p,n)^{14}N, and ^{14}N(γ,π^+)^{14}C reactions. Although the $L=0$ transition amplitude is found to be relatively small, it is not small enough to give quantitative agreement with the severely retarded ^{14}C β-decay rate. The possibility that the vanishingly small β-decay matrix element is the result of destructive interference between the one-body matrix element and other terms is discussed.

I. INTRODUCTION

The $A=14$ system has long been a testing ground for models of nuclear structure and the nucleon-nucleon force. The focus of many of these studies has been the ^{14}N ground state ($J^\pi=1^+$, $T=0$) and the isospin triplet consisting of the ^{14}C ground state, the ^{14}N 2.313 MeV state, and the ^{14}O ground state ($J^\pi=0^+, T=1$). The considerable speculation about these states[1–13] has been fueled by the anomalously retarded β decay of the ^{14}C ground state. Most of these studies have assumed that retardation is due to a nearly complete cancellation among terms in the one-body β-decay matrix element. A number of wave functions have been proposed which not only satisfy this requirement, but are also consistent with other observed static and low-momentum transfer properties of the $A=14$ system.[2–5,11–14]

The well-understood electron scattering reaction provides a clear test for the reliability of these wave functions. Indeed, if a $1p$-shell structure is assumed for these states, the shell model configuration amplitudes can be deduced phenomenologically from the data[15–17] on the magnetic dipole form factors for the ^{14}N ground state and for the transition to the 2.313 MeV 0^+ level. Although such analyses[15] give wave functions for the ^{14}N ground state that are in accord with conventional $1p$-shell structure models, the results for the 2.313 MeV 0^+ level are unexpected. The dominant component in the wave function for the 2.313 MeV level is found not to be the $|1p_{1/2}^{-2}\rangle$ configuration, but instead the $|1p_{3/2}^{-2}\rangle$ configuration. In the case of the 2.313 MeV transition, this leads to smaller $L=2$ transition amplitudes than given by previous models. Although the (e,e') results are not particularly sensitive to the $L=0$ component in the 2.313 MeV transition, the $L=0$ transition amplitude is found to be small, in qualitative but not quantitative agreement with the highly suppressed β decay: The deduced one-body β-decay matrix element is still nearly 2 orders of magnitude larger than the observed value. If this deduced $L=0$ transition amplitude is correct, the vanishingly small β-decay matrix element must arise through destructive interference between the one-body term and contributions from normally negligible processes such as meson exchange currents,[18,19] core polarization, or relativistic effects.

Since such an interpretation differs from the traditional description, it is also important to assess measurements made using other reactions.[20–36] The principal objectives here are twofold: to seek confirmation of the reduction in the $L=2$ strength, and more importantly, to search for a more definitive determination of the $L=0$ strength. Of particular interest are measurements of inelastic proton scattering at intermediate energies ($E_p > 100$ MeV) and forward angles,[26,30] where the scattering amplitude is dominated by the $L=0$ central interaction and thus is nearly proportional to the one-body β-decay matrix element.[37] Consequently, if the suppression of the β-decay rate is the result of a small one-body matrix element, then

small cross sections should be measured in (p,p') at low momentum transfers where the $L=0$ central amplitude is normally dominant. Although alternative interpretations have been advanced,[29,30] the sizable forward angle strength in fact observed in (p,p') measurements could be indicative of nonzero $L=0$ strength.

The ^{14}C(p,n)^{14}N reaction at intermediate energies should also provide information on the magnitude of the $L=0$ strength, and has additional advantages in that it proceeds through the same $\sigma\tau$ operator that mediates the ^{14}C β decay, and also involves the same initial and final states.

Perhaps of even greater relevance though is the reaction[35,36] ^{14}N(γ,π^+)^{14}C, for which the reaction mechanism is better understood than in (p,p') or (p,n). The threshold photopion production operator involves only the spin- and isospin-flip operators, and is less complicated than electron scattering. Pion production at forward angles should therefore be particularly revealing insofar as the $L=0$ strength is concerned.

We begin by briefly describing in Sec. II the experimental details of the electron scattering measurements. The previous analyses of the structure of the 1^+0 and 0^+1 levels are then summarized in Sec. III. Our analysis using the (e,e') measurements is discussed in Sec. IV. Then in Secs. V, VI, and VII, our analysis is applied to the (p,p'), (p,n) and (γ,π^+) reactions, respectively. Finally, in Sec. VIII we present out conclusions and discuss the relationship of our results to the question of the very strongly retarded β decay of ^{14}C.

II. EXPERIMENTAL METHOD AND DATA ANALYSIS

The measurements of electron scattering from ^{14}N were made at the Bates Linear Accelerator Center using a high resolution magnetic spectrometer. Details of this facility have been well documented elsewhere,[38,39] so little elaboration is needed here. Incident electron energies were in the range 80.0—372.6 MeV. For all incident energies except 372.6 MeV, measurements were made at a scattering angle of 180°, using the special deflection system constructed by Peterson *et al.*[40] The scattering angle was 150° for the 372.6 MeV measurement.

For the measurements at 248 and 277 MeV, two solid boron nitride (BN) targets (53.5% nitrogen, 42.5% boron, 4% impurities), machined to mass thicknesses of 203.2 and 457.2 mg/cm^2 were used. However, at 332 and 373 MeV, only the thicker BN target gave adequate counting rates. Gaseous N_2 was used as the target material for incident energies below 240 MeV.

The gas targets[41] consisted of two cylindrical cells 10 cm in length with entrance and exit windows of 24 μm Havar foil. The gas pressure and temperature in each cell were monitored by a pressure transducer and a platinum resistance thermometer. This provided a continuous measurement of the target thickness. In addition, each cell was cooled by an internal coil circulating alcohol at $\sim$0 °C for thermal stability. One cell was filled with natural N_2 gas (99.63% ^{14}N) to give a ^{14}N thickness of $\sim$70 mg/cm^2. The second cell held either H_2 gas, with a thickness of $\sim$2.5 mg/cm^2, or ^{20}Ne gas, with a thickness of $\sim$50 mg/cm^2. The ^{20}Ne was used at energies between 80 and 110 MeV as a check on the Coulomb ($C0$) contamination in the ^{14}N elastic peak. The overall normalization of the measured cross sections was determined by measuring the proton elastic cross section for which the absolute value is well known.[42] For the gas target runs, this was obtained from measurements using the H_2 filled target. When BN targets were utilized, the normalization measurements were made on polyethylene (CH_2) targets.

The use of gas target cells complicated the analysis of the data. For example, the entrance and exit foils contributed an energy-dependent background which was estimated by making separate measurements on Havar foils at each spectrometer setting. The foil data were smoothed by a five-point smoothing procedure to reduce statistical fluctuations and the resultant spectra were subtracted from the ^{14}N spectra channel by channel. Corrections were also made for the effects of localized heating of the target gas, which decreased the effective target thickness. Based on the measurements of Singhal[43] for ^{15}N gas targets, the decrease in the thickness is $\sim$1% for each 5 μA of average beam current and amounted to $\sim$3% for the ^{14}N and ^{20}Ne measurements. No correction was made to the H_2 measurements as the temperature relaxation of the H_2 gas occurs quickly enough to disperse local hot spots.

Experimental cross sections were extracted by line shape fitting the measured spectra. The procedure includes corrections for soft-photon emission, thick-target bremsstrahlung, and Landau straggling to account for radiative and ionization losses. Details of the procedure may be found in Ref. 44. The elastic cross section was corrected for longitudinal $C0$ and $C2$ elastic scattering contributions. The $C0$ corrections accounted for up to 50% of the cross section observed at the lowest energies, but by 162 MeV had decreased to less than 0.1%. At incident energies less than 120 MeV, this contribution was determined by measuring the pure $C0$ ^{20}Ne elastic cross section. This was then scaled by the ratio of ^{14}N to ^{20}Ne cross sections calculated in the distorted-wave Born approximation (DWBA) using the known ground state charge densities.[17,45] In effect, this procedure calibrated the effective scattering angle,[43] which was always 1°—2° less than 180°. At energies above 120 MeV the $C0$ contribution was not measured separately but simply calculated from the known ^{14}N charge density. At all energies the $C2$ contributions were estimated from the $C2$ form factors deduced from forward angle scattering measurements[17] and were less than 1% of the measured cross sections. Finally, corrections were made for $M1$ elastic scattering from the 0.37% natural abundance of ^{15}N in the natural N_2 gas. As estimated from the data of Singhal *et al.*,[43] these corrections ranged from less than 0.5% for the lowest energies to $\sim$5% at 225 MeV. In the measurements made using the BN targets, the corrections for ^{15}N $M1$ scattering ranged to 12%, while the $C0$ contributions were less than 1.2% and the $C2$ contributions less than 0.2%.

The measured $M1$ cross sections and form factors are given in Table I. The form factors are defined relative to the cross sections as in Ref. 15. In order to approximately account for distortion of the incident and scattered elec-

TABLE I. Experimental $M1$ electron scattering cross sections for elastic scattering and for the transition to the level at 2.313 MeV. The number in square brackets refers to the power of 10, i.e., [−5] denotes $\times 10^{-5}$.

E_0 (MeV)	Angle (deg)	q (fm^{-1})	q_{eff} (fm^{-1})	$d\sigma/d\Omega$ (nb/sr)	F_T^2	Error (%)
			^{14}N, 0.00 MeV, $(1^+;0)$			
80.0	180.0	0.806	0.850	1.20	3.06[−5]	9.2
90.6	180.0	0.912	0.956	1.13	3.72[−5]	5.8
101.1	180.0	1.017	1.061	1.05	4.30[−5]	6.5
110.8	180.0	1.114	1.158	8.50[−1]	4.18[−5]	4.7
135.3	180.0	1.357	1.402	5.16[−1]	3.80[−5]	7.0
162.8	180.0	1.630	1.674	2.02[−1]	2.16[−5]	5.1
164.8	180.0	1.650	1.694	1.67[−1]	1.83[−5]	7.0
181.0	180.0	1.810	1.854	1.07[−1]	1.41[−5]	6.8
224.2	180.0	2.235	2.279	1.91[−2]	3.91[−6]	23.2
248.4	180.0	2.471	2.515	8.56[−3]	2.16[−6]	10.4
277.1	180.0	2.751	2.795	2.09[−3]	6.59[−7]	14.6
331.9	180.0	3.282	3.326	1.18[−4]	5.38[−8]	29.4
			^{14}N, 2.313 MeV, $(0^+;1)$			
80.0	180.0	0.794	0.838	1.12	2.86[−5]	5.4
90.6	180.0	0.900	0.944	1.06	3.46[−5]	4.1
101.1	180.0	1.005	1.049	9.70[−1]	3.96[−5]	6.6
110.8	180.0	1.102	1.146	9.97[−1]	4.90[−5]	4.0
135.3	180.0	1.346	1.390	7.63[−1]	5.61[−5]	4.9
162.8	180.0	1.619	1.662	4.01[−1]	4.29[−5]	4.6
164.8	180.0	1.638	1.682	3.73[−1]	4.08[−5]	5.4
181.0	180.0	1.798	1.842	2.82[−1]	3.73[−5]	4.4
224.2	180.0	2.223	2.267	7.73[−2]	1.58[−5]	9.7
277.1	180.0	2.740	2.784	1.42[−2]	4.48[−6]	10.3
331.9	180.0	3.271	3.315	2.38[−3]	1.08[−6]	5.9
372.6	150.0	3.545	3.587	9.22[−4]	4.78[−7]	15.0

tron waves, we tabulate these form factors as a function of the effective momentum transfer,[43] q_{eff}:

$$q_{\text{eff}}=q[1+3\sqrt{3}Ze^2/(2\sqrt{5}\langle r^2\rangle^{1/2}E_0)] ,$$

where $\langle r^2\rangle$ is the mean square charge radius and E_0 is the incident electron energy.

III. PREVIOUS ANALYSES

Following the suggestion of Inglis,[1] the basis space for most of the previous analyses has been limited to the $1p$ shell. Inglis showed that the cancellation necessary in the one-body β-decay matrix element could be achieved within the limited $1p$-shell space if a tensor component was included along with the central and spin-orbit forces in the nucleon-nucleon potential. (Without the tensor force, he concluded that even the inclusion of $2s$ $1d$-shell admixtures in the wave function was unable to provide the necessary cancellation in the matrix element. Subsequent calculations by True,[8] which included $2s$ $1d$-shell configurations and employed only central and spin-orbit terms, confirmed this conclusion. Although True's calculations gave a good description of the ^{14}N energy level scheme up to 10.50 MeV, Rose, Hausser, and Warburton[10] showed that the wave functions were unable to provide the necessary cancellation in the β-decay matrix element, or the correct gamma-ray decay width.)

Accordingly, the analyses presented in this paper employ a $1p$-shell space to describe the ground and 2.313 MeV states in ^{14}N with no restriction on the form of the force to be used in this basis. The wave functions are constructed by coupling two $1p$-shell holes to a filled $1p$ shell, i.e., an ^{16}O core. In a j-j coupling description, the most general wave functions are

$$|J^\pi=1^+, T=0\rangle=a\,|1p_{1/2}^{-2}\rangle+b\,|1p_{3/2}^{-1},1p_{1/2}^{-1}\rangle + c\,|1p_{3/2}^{-2}\rangle , \quad (1)$$

$$|J^\pi=0^+, T=1\rangle=m\,|1p_{1/2}^{-2}\rangle+n\,|1p_{3/2}^{-2}\rangle , \quad (2)$$

where the configuration amplitudes are normalized by

$$a^2+b^2+c^2=m^2+n^2=1 . \quad (3)$$

For wave functions of this form, the static properties of the $A=14$ system relevant to the present discussion are the following.

(1) The ^{14}N ground state magnetic dipole moment,

$$\mu=\tfrac{1}{3}(1.12a^2+0.76ab+2.07b^2 -0.38\sqrt{10}bc+1.88c^2)\,\mu_N . \quad (4)$$

(2) The ^{14}N ground state electric quadrupole moment,

TABLE II. $1p$-shell configuration amplitudes for the wave functions of the ground and 2.313 MeV states given by previous investigators.

	Expt.[a]	j-j coupl. limit	$^3S_1$ L-S coupl. limit	$^1P_1$ L-S coupl. limit	JT[b]	Elliot[c]	VF[d]	SGHH[e]	CK (8-16)2BME[f]	CK POT[f]	Ensslin[g]
a		1.000	−0.192	0.471	0.890	0.914	0.926	0.896	0.949	0.976	0.676
b		0.000	−0.770	0.471	−0.410	−0.397	−0.362	−0.286	−0.313	−0.206	−0.735
c		0.000	0.609	0.745	0.197	−0.087	0.119	0.344	−0.027	−0.076	−0.054
m		1.000	0.577	0.577	0.99	0.949	0.967	0.966	0.923	0.914	0.760
n		0.000	0.817	0.817	0.09	0.315	0.250	0.259	0.384	0.405	−0.651
μ (μ_N)	0.404	0.373	0.88	0.5	0.377	0.320	0.352	0.405	0.326	0.331	0.403
Q (mb)	15.6	0.0	0.0	−1.27	10.6	9.9	9.6	6.6	8.12	5.21	15.8
β decay ($\times 10^{+3}$)	±0.83	−333.0	1000	0.0	6.9	0.0	0.0	0.0	−50.0	−155.0	0.0
$10^{15}T_m$ (s)	92±10	8.01	0.294	9.74	27.0	39.5	28.2	24.0	140.3	112.1	70.4

[a]Reference 46.
[b]Jancovici-Talmi, Ref. 2.
[c]Reference 4.
[d]Visscher-Ferrell, Ref. 5.
[e]Sherr *et al.*, Ref. 3.
[f]Reference 14.
[g]Reference 12.

$$Q=(\langle r^2\rangle/5)(-2ab+b^2/2-\sqrt{2/5}bc-\tfrac{4}{5}c^2)\ , \tag{5}$$

where $\langle r^2\rangle^{1/2}=2.524$ fm is the root mean square radius.[17]

(3) The radiative lifetime of the 2.313 MeV state,

$$T_m=\frac{[9\hbar(M_Nc^2)^2/E_x^3](\hbar c/e^2)}{[-2.71am-8.42bm-4.21\sqrt{2}bn+5.71\sqrt{5}cn]^2}\ , \tag{6}$$

where M_N is the nucleon mass and E_x is the excitation energy.

(4) The $^{14}C(\beta^-)^{14}N$ Gamow-Teller matrix element,

$$\langle J^\pi=1^+, T=0||\sigma\tau||J^\pi=0^+, T=1\rangle = -2(am+2bm+\sqrt{2}bn-\sqrt{5}cn)\ . \tag{7}$$

In other $1p$-shell studies, Jancovici and Talmi,[2] Elliot,[4] and Visscher and Ferrell[5] examined further the effect of various parametrizations of the nuclear two-body force. Each of these investigations was constrained by the requirements that the calculated one-body ^{14}C β-decay matrix element be close to zero and that the ^{14}N ground state dipole and quadrupole moments be approximately correct. The deduced $1p$-shell configuration amplitudes from these three investigations are very similar.

A more general approach was later adopted by Cohen and Kurath,[14] who obtained $1p$-shell two-body potential matrix elements by fitting energy levels for nuclei throughout the $1p$-shell. In other $1p$-shell nuclei, the wave functions derived from the Cohen-Kurath two-body matrix elements have been reasonably successful in describing observed experimental properties, including electron scattering form factors. (As will be seen below, however, these wave functions appear to be less appropriate for the 2.313 MeV level in ^{14}N.)

In contrast, Sherr *et al.*[3] and Ensslin and collaborators[11,12] have taken strictly phenomenological approaches. Sherr *et al.* used the normalization conditions [Eq. (3)], the two ground state moments [Eqs. (4) and (5)], and the β-decay matrix element [Eq. (7)] to determine the configuration amplitudes. Ensslin *et al.* measured the electron scattering $M1$ form factor for the 2.313 MeV transition in the momentum transfer range 0.61–1.16 fm^{-1}. Configuration amplitudes were then deduced, using as constraints the measured form factor along with the magnetic moment, the β-decay matrix element (assumed to be zero), and the normalization conditions.

Table II summarizes the results of the above studies and includes the values obtained for the properties of the $A=14$ system. For comparison, the j-j and L-S coupling limits are also given.

IV. INTERPRETATION OF THE ELECTRON SCATTERING FORM FACTORS

Using harmonic oscillator single-particle wave functions in a $1p$-shell basis, the magnetic dipole form factors for elastic scattering and for the excitation of the 2.313 MeV state in ^{14}N take the form[47,48]

$$F_{el}(q)=(qe^{-y}/Z)(A_0+A_1y)f_{SN}f_{c.m.}\ , \tag{8}$$

$$F_{in}(q)=(qe^{-y}/Z)(B_0+B_1y)f_{SN}f_{c.m.}\ , \tag{9}$$

where $y=q^2b_0^2/4$, with b_0 the oscillator parameter. The functions $f_{c.m.}$ and f_{SN} are the center-of-mass[49] and nucleon-finite-size[50] corrections. The terms A_0, A_1, B_0, and B_1 can be written as functions of the amplitudes a, b, c, m, and n:

$$A_0=(\tfrac{4}{3})^{1/2}(\hbar c/2M_Nc^2)\mu(\mu_N) =(\hbar c/3\sqrt{3}M_Nc^2)(1.12a^2+0.76ab+2.07b^2 -0.38\sqrt{10}bc+1.88c^2)\ , \tag{10a}$$

$$A_1=(\hbar c/3\sqrt{3}M_Nc^2)(1.76a^2-0.88ab-1.32b^2+0.44\sqrt{10}bc-0.704c^2)\ , \quad (10b)$$

$$B_0=-(\hbar c/3\sqrt{6}M_Nc^2)\{9[\hbar(M_Nc^2)^2/E_x^3](\hbar c/e^2)/T_m\}^{1/2}$$
$$=-(\hbar c/3\sqrt{6}M_Nc^2)(2.71ma+8.42mb+4.21\sqrt{2}nb+5.71\sqrt{5}nc)\ , \quad (10c)$$

$$B_1=(\hbar c/3\sqrt{6}M_Nc^2)(9.4ma+4.7mb+2.35\sqrt{2}nb-3.76\sqrt{5}nc)\ . \quad (10d)$$

The form factors calculated using the Cohen-Kurath matrix element sets (8-16)2BME and (8-16)POT are shown in Fig. 1. These form factors are very similar to those obtained using the wave functions of earlier investigators[2,4,5] since the configuration amplitudes are nearly the same. The measured elastic form factor is reasonably well described, the calculations having approximately the correct shape and magnitude. On the other hand, the description of the observed inelastic form factor is much poorer. The calculation appears to have the correct shape for momentum transfers below 1.5 fm^{-1}; however, it exceeds the data by a factor of 3 in magnitude. A further difficulty is that the calculated form factors have the wrong shape at high q, falling off much faster than the measurements.

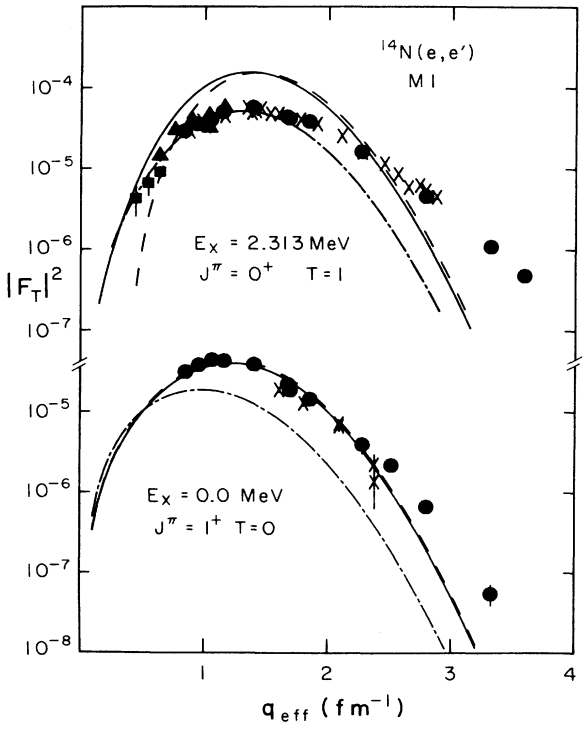

FIG. 1. $M1$ form factors measured for the ground state [● this experiment; ×, Mainz (Ref. 15)] and 2.313 MeV transition (▲, Ref. 12; ■, Ref. 16; ×, Refs. 15 and 17; ●, this experiment) in ^{14}N. The data are compared to the results of calculations using the wave functions of Cohen and Kurath (Ref. 14) [(8-16)2BME, solid curves; (8-16)POT, dashed curves] and of Ensslin *et al.* (Ref. 12) (dashed-dotted curves).

In contrast, as also shown in Fig. 1, the direct fitting of the low-q electron scattering data for the 2.313 MeV transition by Ensslin *et al.*[11,12] results in an inelastic form factor in accord with the data, at least to $q=1.5$ fm^{-1}. However, the elastic form factor calculated with the amplitudes of Ensslin *et al.* describes the data poorly, underpredicting the measured form factor by a factor of 2 at the maximum.

As a first step in the investigation of the source of these discrepancies, we have calculated the contributions from meson exchange currents (MEC). Since there is no contribution in lowest order to the isoscalar ($\Delta T=0$) elastic form factor, these effects clearly are unable to explain the deficiencies of the Ensslin wave functions. For the inelastic wave function, the MEC contributions calculated with Cohen-Kurath wave functions amount to an enhancement of ~25% at the maximum of the form factor and of a factor of 2–3 at 3 fm^{-1}. As the Cohen-Kurath model overpredicts the data at the maximum before the MEC effects are considered, their inclusion only exacerbates the discrepancies.

In an attempt to understand why these previous analyses failed to describe both experimental form factors simultaneously, we have adopted an approach similar to that used by Ensslin *et al.*, fitting to the available (e,e') data and other relevant properties. The constraints consisted of both (e,e') form factors (unlike Ensslin, who used only the inelastic result over a more limited momentum transfer region), the normalization conditions, the magnetic dipole moment, and the radiative lifetime T_m of the 2.313 MeV level. The observed β-decay rate was not directly fitted, following the suggestion of Goulard *et al.*[18,19] that the observed retardation may well be due to destructive interference between a small one-body term and terms arising from meson exchange currents. Accordingly, the one-body β-decay matrix element was only constrained to be comparable to the predicted magnitude of the MEC contributions, as much as 2 orders of magnitude larger than the measured matrix element. The ground-state quadrupole moment was also excluded from the fit. It is well known that quadrupole moments are rarely well reproduced in a restricted shell model space; core polarization through multi-$\hbar\omega$ excitations appears to be necessary for agreement. As will be seen, the predicted values of the quadrupole moment differ considerably between the various fits; even the value closest to the experimental one is too small by a factor of 3.

The inelastic (e,e') data set was truncated at $q=2$ fm^{-1}, as it was found that no $1p$-shell model can describe the shape of the 2.313 MeV form factor at high momentum transfer, even when Woods-Saxon single-particle wave functions are used. Such an enhancement of isovector and isovector-dominated $M1$ form factors is a feature observed in a number of nuclei in the $1p$-shell.[43,51–54] Unfortunately, no consistent explanation of this effect has yet been found. A weak enhancement is also seen in the isoscalar elastic form factor. However, in this case there was no obvious need to truncate the data for the purposes of the fit. The processes responsible for the large isovec-

TABLE III. $1p$-shell configuration amplitudes for the wave functions of the ground and 2.313 MeV states deduced in this analysis.

	Expt.[a]	$H1$	$H2$	HF2
a		0.978	0.946	0.974
b		0.071	0.103	−0.228
c		−0.194	0.308	0.000
m		0.553	0.576	0.526
n		−0.833	0.818	0.851
μ (μ_N)	0.404	0.407	0.413	0.334
Q (mb)	15.6	−2.01	−3.64	5.99
β decay ($\times 10^{+3}$)	±0.83	−58.1	−73.1	0.84
$10^{15}T_m$ (s)	92±10	151.5	106.3	96.4
A_0		0.0494	0.0501	0.0405
A_1		0.0635	0.0588	0.0727
B_0		0.0178	0.0212	0.0222
B_1		0.1062	0.1019	0.1032

[a]Reference 46.

tor cross sections observed above $q \cong 2$ fm^{-1} (perhaps core polarization or short-range meson exchange) are assumed to contribute little strength in the lower-q region.[55] In other $1p$-shell nuclei,[43,51–53] the low-q data seem to be well described by wave functions restricted to the $1p$ shell.

The fitting process yielded two solutions, the configuration amplitude sets $H1$ and $H2$, as listed in Table III. Preliminary fits were performed to determine the oscillator radius parameter b_0. The resulting value of $b_0 = 1.72$ fm is close to $b_0 = 1.68$ fm, the value obtained from elastic charge scattering. In the final fits the oscillator parameter was fixed at $b_0 = 1.70$ fm, with the five configuration amplitudes as the only free parameters. Form factors corresponding to set $H1$ are shown in Fig. 2, those for the set $H2$ being nearly identical. The ground state $H1$ and $H2$ wave functions are very similar in structure to those of previous investigators, dominated by the $|1p_{1/2}^{-2}\rangle$ configuration. This is not surprising in that the older wave functions also gave reasonable descriptions of the ^{14}N ground state magnetic moment and $M1$ elastic form factor. The major differences arise in the configuration amplitudes for the 2.313 MeV state. Theoretically based wave functions are almost solely composed of the $|1p_{1/2}^{-2}\rangle$ configuration, with less than 16% $|1p_{3/2}^{-2}\rangle$. The phenomenological amplitudes deduced in the present analysis, which, for $q < 2$ fm^{-1}, provide an improved description of data on the 2.313 MeV transition, give the $|1p_{3/2}^{-2}\rangle$ component as ~70% of the wave function. This result is at odds with the common interpretation that the structure of the $A = 14$ nuclei lies close to the j-j coupling limit. Indeed, the deduced $H2$ configuration amplitudes are almost identical to the L-S coupling limit for the 2.313 MeV state (thus requiring an L-S coupled ground state for ^{14}C).

Since the suggestion of Goulard *et al.*[18,19] concerning the origin of the ^{14}C β-decay rate suppression is open to debate, we have also repeated the above analysis using the decay rate as an explicit constraint. The deduced configuration amplitude set HF2 is listed in Table III and the

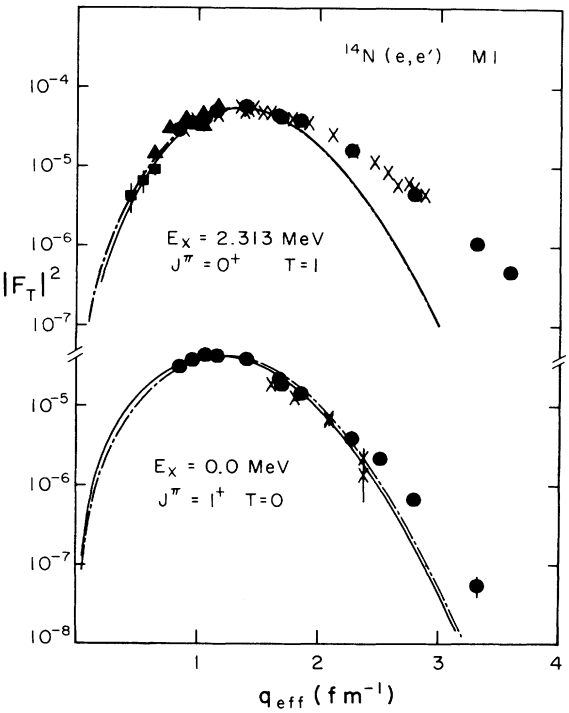

FIG. 2. Experimental $M1$ elastic and 2.313 MeV form factors compared to those calculated with the wave functions of the present analysis. The $H1$ amplitudes give the solid curves and the HF2 amplitudes give the dashed-dotted curves. The $H2$ amplitudes give form factors nearly identical to the $H1$ form factors.

corresponding form factors are shown in Fig 2. The HF2 ground state remains dominated by the $|1p_{1/2}^{-2}\rangle$ configuration and again the 2.313 MeV state is very near the L-S coupling limit. However, as will be seen below, the differences that produce the small one-body β-decay matrix element have important implications for other reactions.

The one-body β-decay matrix element $\langle \sigma\tau \rangle/6$ is related to the spin part of the $L = 0$ component in the (e,e') form factor by

$$F_{\Delta T=1,\Delta L=0}(q) = (-\hbar c/3\sqrt{6}M_N c^2) \times (qe^{-y}/Z)(\mu_1\langle \sigma\tau \rangle/2 + \langle \text{current} \rangle) \times (1-2y/3) f_{SN} f_{\text{c.m.}} ,$$

where $\mu_1 = 4.71\mu_N$. In terms of the $1p$-shell description given above, the convection current matrix element is given by

$$\langle \text{current} \rangle = 2am + bm + \sqrt{2}bn/2 + \sqrt{5}cn .$$

Unfortunately, the $L = 0$ component is not directly determined by the fits to the (e,e') data. Figure 3 shows the decomposition of the best-fit form factors into $L = 0$ and 2 components. As can be seen, the $L = 0$ contribution can be modified appreciably without compromising the overall fit. The data are primarily sensitive to the $L = 2$ term and it is only this part of the transition density that

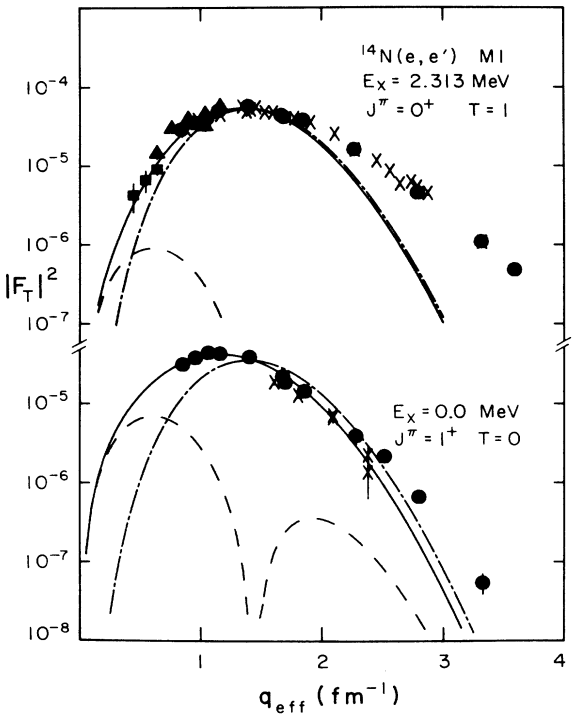

FIG. 3. Decomposition of the $H1$ form factors into $L=0$ (dashed curve) and $L=2$ (dashed-dotted curve) contributions.

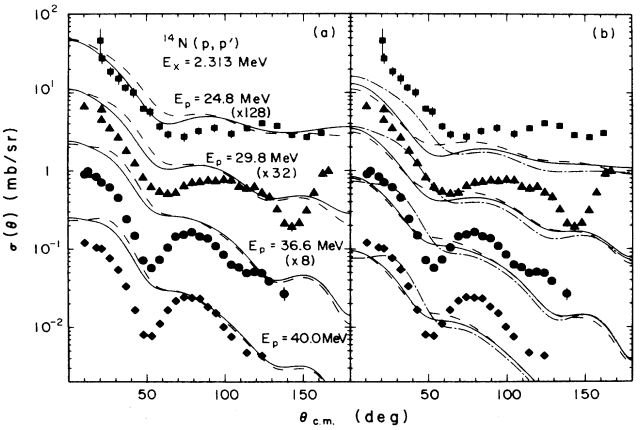

FIG. 4. Differential cross sections for the ^{14}N(p,p') (2.313 MeV) reaction for $E_p=24.8$, 29.8, 36.6, and 40.0 MeV and comparison with calculations using the M3Y force of Love (Refs. 57 and 58). In (a) the wave function amplitudes of Cohen and Kurath (Ref. 14) [(8-16)2BME], solid curve, and of Visscher and Ferrell (Ref. 5), dashed curve, are used. In (b) the calculations employ the amplitudes $H1$ (solid curve), $H2$ (dashed curve), and HF2 (dashed-dotted curve). The data are from Refs. 21 and 27.

is reliably determined.

It should be emphasized, however, that the restriction of the analysis to a $1p$-shell space plays an important role by correlating the various transition amplitudes. The five configuration amplitudes a, b, c, m, and n are subject to the normalization conditions of Eq. (3), thus leaving only *three* free parameters. To the extent that the elastic scattering determines the two remaining parameters of the ground state, there remains only *one* free parameter to fit the transition to the 2.313 MeV level. Consequently, if the electron scattering determines the $(L=2; S=1)$ transition amplitude, it in effect determines the one remaining wave function amplitude. The (0;1), (1;0), and (1;1) transition amplitudes are then completely specified [except for choices of sign in applying Eq. (3)]. While, in fact, our global fitting procedure also allows the inelastic data to influence the ground state parameters, the point remains that the four L-S—coupling transition amplitudes describing the inelastic transition *are not independent quantities*, but are interrelated by the $1p$-shell model.

V. PROTON SCATTERING AND THE EXCITATION OF THE 2.313 MeV STATE IN ^{14}N

As in the case of electron scattering, the $L=0$ central interaction amplitude for inelastic proton scattering is nearly proportional to the one-body β-decay matrix element.[37] Consequently, the suppressed β-decay matrix element implies that small cross sections should also be measured in (p,p') at small momentum transfers where the $L=0$ central amplitude is normally dominant. Although there have been many (p,p') studies of the ^{14}N 2.313 MeV transition,[20–30] theoretical analyses reproduce only qualitatively the measured (p,p') angular distributions. Since the analysis of data obtained at incident proton energies $E_p<15$ MeV is obscured by effects such as compound nucleus formation,[25] the following discussion will focus on measurements made using protons with energies above 20 MeV,[21,26–30] where the direct reaction is expected to dominate.

Shown in Fig. 4(a) are the data of Crawley *et al.*[21] ($E_p=24.8$ MeV) and Fox and Austin[27] ($E_p=29.8$, 36.6, and 40.0 MeV). For these relatively low incident proton energies the forward-angle peaks in the cross sections are due to the $L=2$ amplitude with equal contributions from the central force and the tensor force. The $L=0$ central amplitude makes a lesser contribution, and so these measurements are not strongly correlated with the magnitude of the β-decay matrix element. Figure 4(a) also shows distorted wave impulse approximation (DWIA) calculations performed using the computer code DWBA70,[56] with the M3Y effective interaction[57] of Love[58] and optical potentials of Fox and Austin.[27] The transition densities were obtained from wave functions of Visscher and Ferrell[5] and Cohen and Kurath[14] [(8-16)2BME]. As may be observed, both sets of wave functions reproduce the trend of the data at forward scattering angles. Nevertheless, it is admitted that the M3Y interaction does not predict the forward angle peak with the same quantitative accuracy as the somewhat arbitrary phenomenological "$\sqrt{f}(S+LS+1.25$ OPEP)" force used by Fox and Austin[27] to describe these data (OPEP denotes one-pion exchange potential). As will be seen, however, this is no longer the case when more realistic wave functions are

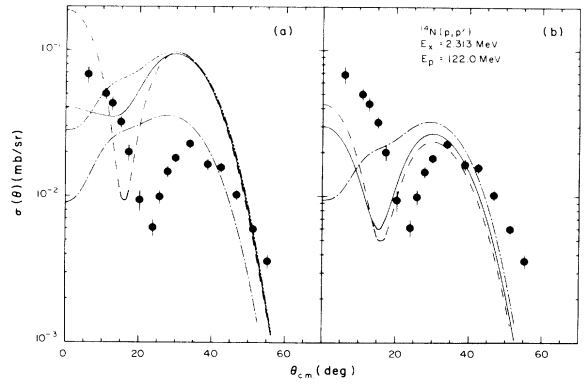

FIG. 5. Differential cross sections for the ^{14}N(p,p') (2.313 MeV) reaction for $E_p = 122$ MeV. In (a) the curves show the results of calculations using the Cohen-Kurath (8-16)2BME wave functions (Ref. 14) (solid curve), the Cohen-Kurath (8-16)POT wave functions (Ref. 14) (dashed curve), the wave functions of Ensslin *et al.* (Ref. 12) (dashed-dotted curve), and the Visscher-Ferrell wave functions (Ref. 5) (dashed—double-dotted curve). The calculations in (b) use the wave function amplitudes $H1$ (solid curve), $H2$ (dashed curve), and HF2 (dashed-dotted curve). The data are from Ref. 26.

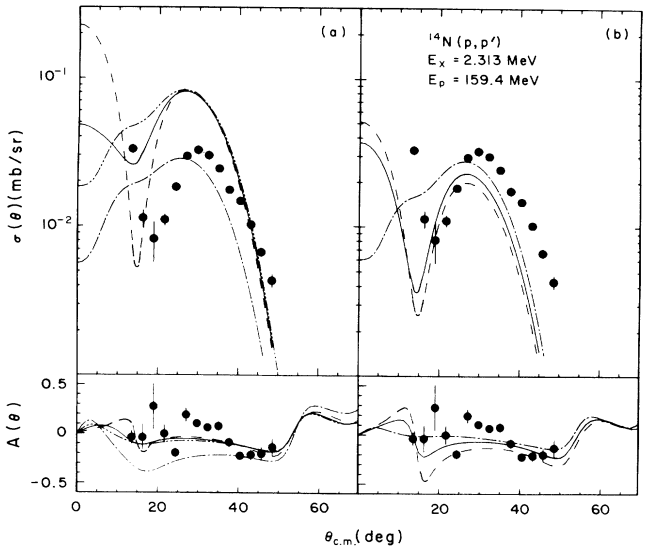

FIG. 6. Differential cross sections and analyzing powers for the ^{14}N(p,p') (2.313 MeV) reaction for $E_p = 159.4$ MeV. The calculations in (a) use the Cohen-Kurath (8-16)2BME wave functions (Ref. 14) (solid curve), the Cohen-Kurath (8-16)POT wave functions (Ref. 14) (dashed curve), the wave functions of Ensslin *et al.* (Ref. 12) (dashed-dotted curve), and the Visscher-Ferrell wave functions (Ref. 5) (dashed—double-dotted curve). In (b) the wave function amplitudes $H1$ (solid curve), $H2$ (dashed curve), and HF2 (dashed-dotted curve) are used. The data are from Ref. 30.

used.

Figures 5(a) and 6(a) show the intermediate energy data of Comfort *et al.*[26] ($E_p = 122$ MeV) and Taddeucci *et al.*[30] ($E_p = 159.4$ MeV). These data are compared to the results of DWIA calculations using the effective interactions of Love and Franey[59] (140 and 175 MeV t matrix), optical potentials of Comfort *et al.*[26] (122 MeV) and Taddeucci *et al.*[30] (159.4 MeV), and wave functions of Cohen and Kurath,[14] Visscher and Ferrell,[5] and Ensslin *et al.*[12] At these higher proton energies, the peak observed at forward scattering angles can be attributed to the $L = 0$ central interaction. The two sets of Cohen-Kurath wave functions are reasonably consistent with this peak, but as noted in Table II, they overpredict the β-decay matrix element by approximately 2 orders of magnitude. On the other hand, the wave functions of Visscher and Ferrell and Ensslin *et al.*, which are tailored to fit the suppressed β-decay rate, do not account for the forward angle strength in the (p,p') data. Only the wave functions of Ensslin *et al.* are able to provide a reasonably quantitative description of the second maximum near 30°, which is of $L = 2$ character. The other wave functions give differential cross sections for this peak which are too large by a factor of about 3.

The failure of these analyses to account for the (p,p') data on the 2.313 MeV transition is not surprising since the wave functions used also failed to describe the electron scattering results. We have therefore recomputed the differential (p,p') cross sections and analyzing power angular distributions using the new $H1$, $H2$, and HF2 wave functions. In the j-j coupled representation, the particle-hole spectroscopic coefficients Z_J^τ(p,h) required by DWBA70 are related to the one-body transition density matrix elements $\psi_{J\tau}^{fi}(j_p, j_h)$ by

$$Z_J^\tau(\mathrm{p,h}) = (-1)^{T_i - M_{T_i}} \langle T_f M_{T_f} T_i - M_{T_i} \mid \tau M \rangle \times \psi_{J\tau}^{fi}(j_p, j_h)/(\hat{J}_i) ,$$

where J is the spin transfer, τ is the isospin transfer, $\hat{J}_i = (2J_i + 1)^{1/2}$, and

$$\psi_{J\tau}^{fi}(j_p, j_h) = \langle J_f T_f || (a_{j_p}^\dagger \times a_{j_h})^{J\tau} || J_i T_i \rangle / (\hat{J})(\hat{\tau}) .$$

For the $1p$-shell model described earlier, these one-body density matrix elements are

$$\psi_{11}^{0^+1\,1^+0}(\tfrac{1}{2}, \tfrac{1}{2}) = -am ,$$

$$\psi_{11}^{0^+1\,1^+0}(\tfrac{3}{2}, \tfrac{3}{2}) = -cn/\sqrt{2} ,$$

$$\psi_{11}^{0^+1\,1^+0}(\tfrac{3}{2}, \tfrac{1}{2}) = -bm/\sqrt{2} ,$$

$$\psi_{11}^{0^+1\,1^+0}(\tfrac{1}{2}, \tfrac{3}{2}) = bn/2 .$$

The spectroscopic factors may be transformed into an L-S coupled basis using

$$Z_J^\tau(LS) = \sum_{j_p j_h} (\hat{j}_p \hat{j}_h \hat{L} \hat{S}) \begin{Bmatrix} l_p & \frac{1}{2} & j_p \\ l_h & \frac{1}{2} & j_h \\ L & S & J \end{Bmatrix} Z_J^\tau(\mathrm{p,h}) .$$

TABLE IV. Spectroscopic factors for the $(1^+0)\rightarrow(0^+1)$ transition.

	CK(8-16)POT[a]	CK(8-16)2BME[a]	Ensslin[b]	VF[c]	$H1$	$H2$	HF2
Z_j^τ(p,h)							
$Z_1^1(1p_{1/2},1p_{1/2})$	−0.515	−0.506	−0.297	−0.518	−0.312	−0.315	−0.296
$Z_1^1(1p_{3/2},1p_{3/2})$	0.013	0.004	−0.014	−0.012	−0.066	−0.103	0.000
$Z_1^1(1p_{1/2},1p_{3/2})$	−0.024	−0.035	0.138	−0.026	−0.017	0.024	−0.056
$Z_1^1(1p_{3/2},1p_{1/2})$	0.077	0.118	0.228	0.143	−0.016	−0.024	0.049
$Z_j^\tau(LS)$							
$Z_1^1(01)$	0.052	0.017	0.000	0.000	0.019	0.024	0.000
$Z_1^1(21)$	−0.477	−0.483	−0.279	−0.494	−0.251	−0.228	−0.287
$Z_1^1(11)$	0.037	0.059	0.259	0.082	−0.023	0.000	−0.005
$Z_1^1(10)$	−0.200	−0.185	−0.121	−0.197	−0.196	−0.241	−0.104

[a]Reference 14.
[b]Reference 12.
[c]Reference 5.

In this representation, the transition amplitudes $Z_1^1(01)$ and $Z_1^1(21)$ determine the amounts of $L=0$ and $L=2$ strength in the direct (p,p′) amplitude. The one-body β-decay matrix element is nearly proportional to the amplitude $Z_1^1(01)$. Table IV lists Z_j^τ(p,h) and $Z_j^\tau(LS)$ for the older wave functions[5,12,14] as well as the phenomenological $1p$-shell wave functions $H1$, $H2$, and HF2. As discussed above, these spectroscopic factors are not completely independent within the context of a $1p$-shell model.

The calculations for $E_p=20$–40 MeV are shown in Fig. 4(b). Since the dominant term is the $L=2$ component, all three wave functions, which have similar $Z_1^1(21)$ contributions, give similar results. In comparison to the calculations shown in Fig. 4(a), the primary effect is to suppress the overall strength. As a result, the new wave functions give a reasonable description of the forward angle strength for all but the lowest energies. This agreement occurs without the need to reduce the central strength, enhance the tensor contribution, or employ an arbitrary normalization factor, as in the force of Fox and Austin.[27] Indeed, when the Fox-Austin interaction is employed with the new wave functions, the calculations underestimate the observed cross section at small angles by about a factor of 4, for all four incident energies.

The intermediate energy calculations, shown in Figs. 5(b) and 6(b), exhibit the expected strong correlation with the $L=0$ transition amplitude. The differential cross section calculated using HF2 wave functions lacks the peak at small angles since these wave functions were constrained to reproduce the β-decay matrix element and therefore have little $L=0$ strength. The $H1$ and $H2$ wave functions, while overestimating the β-decay rate, do, however, predict forward angle strength in (p,p′). As previously noted, the wave functions having sizable $L=0$ amplitudes ($H1$, $H2$, and Cohen-Kurath) give better descriptions of the forward angle (p,p′) cross sections than wave functions having small $L=0$ amplitudes (Visscher and Ferrell, Ensslin, and HF2). Compared to the predictions of the older wave functions of Cohen and Kurath and Visscher and Ferrell, the new phenomenological wave functions also provide a much better description of the predominately $L=2$ maximum in the (p,p′) data at 30°.

Whereas the use of the new $H1$ and $H2$ amplitudes gives better agreement with the cross section data, none of the amplitude sets is able to reproduce the measured analyzing powers at $E_p=159.4$ MeV. A likely explanation for this is suggested by recent relativistic calculations using a Dirac impulse approximation.[60–62] Compared to standard nonrelativistic calculations, the Dirac formalism gives a much improved description of elastic analyzing powers with only small changes in the calculated cross sections. The ^{14}N(p,p′)^{14}N (2.313 MeV) reaction should constitute an interesting test for such calculations when extended to inelastic scattering.

The need to explain the forward angle strength while preserving the small β-decay matrix element led Taddeucci *et al.*[30] to investigate the possible sensitivity of the calculations to the assumed effective interaction. It was concluded, however, that unreasonably large changes in the interaction would be required in order to obtain the necessary modifications to the differential (p,p′) cross sections and analyzing powers at intermediate energies. A preferred explanation invokes multistep processes in the reaction mechanism. Aoki *et al.*[29] demonstrated that the inclusion of the two-step process (p,d)(d,p′) improves the DWIA description of measurements made at $E_p=21$ MeV. Calculations by Comfort *et al.* at 122 MeV (Ref. 26) and at 160 MeV (Ref. 63) showed that the *elastic* (p,d)(d,p) cross sections are strongly forward peaked and fall off rapidly with increasing angle. It was presumed by Comfort *et al.* that forward peaking would also be characteristic of the *inelastic* two-step processes,[26,30] but quantitative calculations remain to be performed.

VI. THE ^{14}C(p,n)^{14}N REACTION

The (p,n) reaction is generally dominated by the $L=0$ central amplitude and therefore may also provide insight into the $L=0$ strength. For transitions of the type $0^+\leftrightarrow1^+$, it is the $\sigma\tau$ term in the central part of the effective interaction that mediates the reaction. The similarity

between this operator and the Gamow-Teller β-decay operator results in an approximate proportionality between the (p,n) cross section at low momentum transfers and the β-decay rate.[33,34] This correspondence has been exploited by Taddeucci *et al.*,[31,32] who measured the ^{14}C(p,n)^{14}N reaction at $E_p=25$–45 MeV in order to investigate the isospin-dependent central and tensor interactions. Since the ^{14}C(p,n)^{14}N(3.95 MeV; $J^\pi=1^+$, $T=0$) reaction is analogous to a strong Gamow-Teller β decay, the $L=0$ central interaction should dominate the transition through the $\sigma\tau$ operator. On the other hand, the ^{14}C(p,n)^{14}N(g.s) reaction is related to the highly suppressed ^{14}C(β^-) decay with a small $L=0$ contribution. Thus a greater than normal sensitivity to the tensor interaction through the $L=2$ amplitude is expected.

The analysis of the ^{14}C(p,n)^{14}N(g.s) reaction data by Taddeucci *et al.*[31] confirmed these predictions. In particular, features observed in the (p,n) cross section to the ^{14}N ground state indicated the need for a strong tensor interaction; however, reasonable variations in the tensor strength could only provide limited agreement between experiment and theory. While the measured ^{14}C(p,n)^{14}N(g.s) cross section is insensitive to the $L=0$ amplitude and provides little information on the β-decay matrix element, the data may still lend support to the reduced $L=2$ strength in the new phenomenological wave functions. Accordingly, calculations of the ^{14}C(p,n)^{14}N(g.s) reaction have been performed at $E_p=35$ MeV for the new $1p$-shell wave functions, $H1$, $H2$, and HF2, as well as for the older Cohen-Kurath (8-16)2BME (Ref. 14) and Visscher and Ferrell (Ref. 5) wave functions. The calculations, performed using the code DWBA70,[56] employ the optical potentials of Taddeucci *et al.*,[31] and use—for the effective interaction—both the M3Y interaction of Love[57,58] and the force derived by Taddeucci *et al.*[31] The transition is described using spectroscopic amplitudes related to the (p,p') amplitudes by

$$Z_1^1(LS,(\mathrm{p,n}))=(-1)^{L+S}\sqrt{3}Z_1^1(LS,(\mathrm{p,p'}))\ .$$

As shown in Fig. 7, the various calculations give qualitatively similar results, exhibiting large cross sections at low momentum transfer and flattening near 1.1 fm^{-1}, where the data display a diffraction minimum. A notable defect of the calculations is their inability to reproduce the shape of the subsequent maximum observed near $q=1.6$ fm^{-1}. Since the magnitudes of the calculations are governed by the $L=2$ spectroscopic factors, cross sections calculated using wave functions of Cohen and Kurath[14] and Visscher and Ferrell[5] tend to be too large, consistent with our interpretation of the (e,e') and (p,p') reactions. Calculations using the M3Y force together with the new phenomenological wave functions give an approximately correct description of the data below 1 fm^{-1} but, as noted above, fail to reproduce the subsequent maximum. Finally, it should be noted that the differences in cross section shape between the $H1$, $H2$, and HF2 calculations occur primarily through the odd-parity $L=1$ contributions to the exchange amplitudes.

As in the case of (p,p'), for higher incident proton energies the (p,n) cross section at forward angles is more sensitive to the $L=0$ transition amplitude. Fig. 8 shows predicted (p,n) cross sections for $E_p=159.4$ MeV. Except

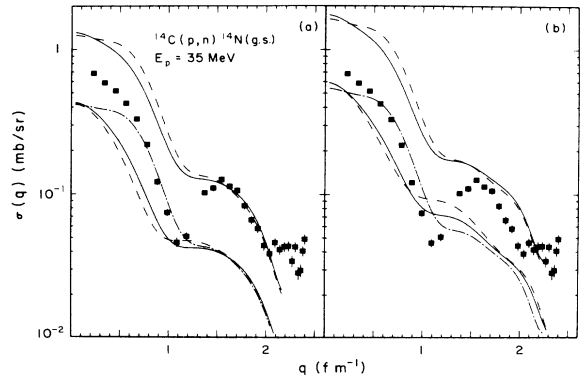

FIG. 7. Differential cross sections for the ^{14}C(p,n)^{14}N(g.s.) reaction for $E_p=35$ MeV. The calculated curves are for the wave functions of Cohen and Kurath (Ref. 14), (8-16)2BME (upper solid curve), and Visscher and Ferrell (Ref. 5) (upper dashed curve), $H1$ (lower solid curve), $H2$ (lower dashed curve), and HF2 (dashed-dotted curve). In (a) the force is that of Taddeucci *et al.* (Ref. 31). In (b) the M3Y force of Love (Refs. 57 and 58) is employed. The data are from Refs. 31 and 32.

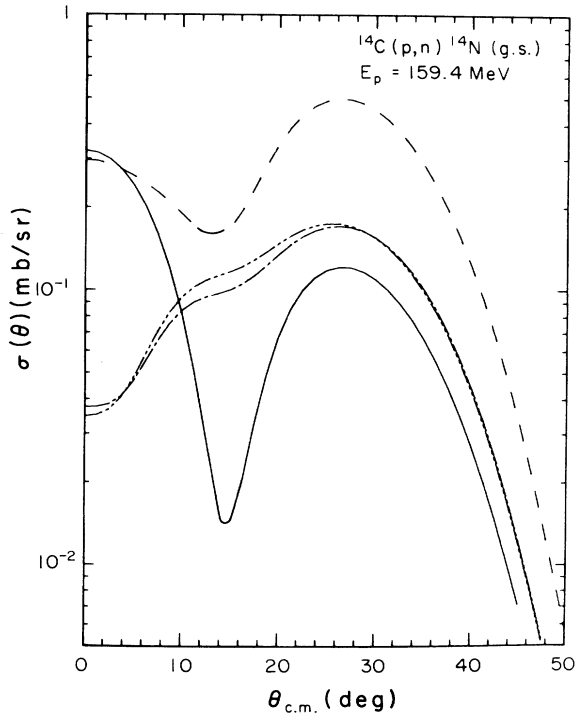

FIG. 8. Differential cross sections for the ^{14}C(p,n)^{14}N(g.s.) reaction for $E_p=159.4$ MeV. The curves show the results of calculations using the wave function amplitudes $H1$ (solid curve), HF2 (dashed-dotted curve), Cohen-Kurath (8-16)2BME (dashed curve), and Ensslin *et al.* (dashed—double-dotted curve).

for an overall normalization factor, a close similarity is seen with the calculated (p,p′) angular distributions shown in Fig. 6.

VII. THE $^{14}N(\gamma,\pi^+)$ REACTION

The photoproduction of low energy pions is a mechanism that is reasonably well understood, and unlike electron scattering, involves only the spin- and isospin-flip operators. Furthermore, the $^{14}N(\gamma,\pi^+)^{14}C$(g.s.) cross sections should be small at low q if the $^{14}C(\beta^-)$ decay rate suppression arises from a direct cancellation in the one-body matrix element. On the other hand, for an $L=0$ transition amplitude of the order of that given by the $H1$ wave functions, the forward angle photopion cross sections should be significantly enhanced over those predicted by wave functions with $Z_1^1(01)=0$.

Figure 9 shows a comparison of pion photoproduction data obtained at incident photon energies of 173 MeV (Ref. 35) and 200 MeV (Ref. 36) with calculations[35,36,64] using the $H1$, $H2$, and HF2 wave functions. The cross sections calculated with the Cohen-Kurath[14] amplitudes are nearly an order of magnitude larger than the $H1$ results at both forward and backward angles and are, therefore, not included in Fig. 9 (see, however, Fig.3 of Ref. 35). Cross sections obtained with the Ensslin[12] wave functions resemble the HF2 results. The 173 MeV data of Rohrich *et al.*[35] clearly differentiate between the various structure models and are in much better agreement with the present phenomenological wave functions than with those of Ensslin[12] or Cohen and Kurath.[14] The 200 MeV data obtained by Cottman and collaborators[36] not only confirm this result but also help discriminate between the $H1$ and $H2$ configuration sets, with $H1$ giving the overall best agreement. In both cases, the data lie in a momentum transfer region where the $L=2$ component of the interaction is important. Thus the (γ,π^+) data provide further evidence for the reduction of the $L=2$ strength in the $0^+\leftrightarrow 1^+$ transition. On the other hand, the calculations shown in Fig. 9 also exhibit a strong sensitivity to the $L=0$ transition amplitude at smaller momentum transfers, a region in which no data presently exist. Current efforts[65] to extend the data into this range should clearly be able to distinguish between the $H1$ (or $H2$) and HF2 (or Ensslin) amplitudes. This will, in turn, provide information crucial for the interpretation of the β decay.

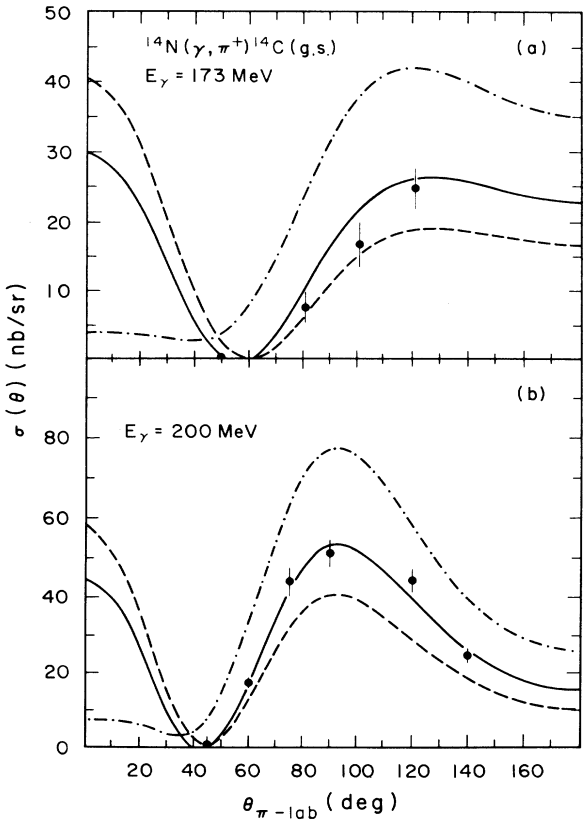

FIG. 9. Differential cross sections for the $^{14}C(\gamma,\pi^+)^{14}N$(g.s.) reaction for (a) $E_\gamma=173$ MeV and (b) $E_\gamma=200$ MeV. The curves show the results of calculations (Refs. 35, 36, and 64) using the wave function amplitudes $H1$ (solid curve), $H2$ (dashed curve), and HF2 (dashed-dotted curve). The data are from Refs. 35 and 36.

It should be noted that one recent pion production measurement for an incident photon energy of 320 MeV (Ref. 66) gives cross sections 3 times greater than those calculated with the $H1$ wave functions. However, for this energy, near the peak of the delta resonance, the Δ term in the photoproduction operator plays a more important role, and the description of the process becomes much more complicated.

VIII. SUMMARY AND CONCLUSIONS

Our electron scattering measurements of the $M1$ form factors for the ^{14}N ground state and transition to the $(0^+;T=1)$ state directly test our understanding of these levels. No previously available models could simultaneously describe both form factors. This inability led us to determine new phenomenological $1p$-shell wave functions which can explain the (e,e′) data to $q\cong 2$ fm^{-1}. The $L=2$ transition amplitude deduced from these wave functions for the 2.313 MeV excitation is reduced by nearly a factor of 2 in comparison to that given by most previous models. This reduction also provides a better overall description of the cross sections measured in (p,p′) and (p,n) reactions at $E_p=24$–45 MeV, (p,p′) reactions at intermediate energies, and (γ,π^+) measurements near threshold.

On the other hand, the (e,e′) measurements do not explicitly determine the $L=0$ transition strength. As previously explained, in the analysis presented here the $L=0$ amplitude is related to the $L=2$ amplitude by restrictions inherent in the assumed $1p$-shell model. More direct information on the $L=0$ component has been sought from intermediate (p,p′) measurements at forward scattering angles. These data show appreciable strength, which, when interpreted literally, suggest a small but nonzero one-body $L=0$ transition amplitude. This result is in qualitative agreement with the $L=0$ strength given by

the $H1$ and $H2$ wave functions determined from the (e,e') data. For a one-body $L=0$ strength of this magnitude, the vanishingly small β-decay matrix element must arise through destructive interference between the one-body matrix element and terms involving normally negligible processes.

Goulard and collaborators[18,19] have suggested that meson exchange currents may be important in this regard. Their results allow us to estimate the MEC contributions to the β-decay matrix element for the new phenomenological wave functions. For the $H1$, $H2$, and HF2 configuration amplitudes, the contributions are -0.032, -0.041, and -0.057. As one can see from Table III, the resulting interference is constructive, not destructive as required. However, since the magnitude of these terms is small, one must also consider other effects, such as those due to relativistic dynamics, core polarization, etc.

It may be many years before a satisfactory understanding of the highly suppressed ^{14}C β-decay rate is achieved. It is crucial to obtain a more definitive measurement of the $L=0$ transition strength. At the present time it appears that the most telling information on the $L=0$ amplitude will come from low energy pion photoproduction measurements at forward angles. Further information on this amplitude may be derived from (p,n) measurements at incident proton energies above 100 MeV. At lower incident energies, $L=2$ terms dominate and there is much uncertainty about the reaction mechanism and the large optical distortion effects. As we have seen, the interpretation of the forward angle (p,p') cross sections, even at intermediate energies, is obscured by a lack of quantitative knowledge regarding two-step processes.

Finally, one important caveat in our analysis must be recognized. The mechanism which gives rise to the enhancement seen at high q in $1p$-shell isovector $M1$ form factors is not understood. Possibilities include core polarization (i.e., configurations outside the $1p$-shell space), non-nucleonic processes, and relativistic effects, but the ultimate explanation is not clear. What is clear, however, is that if this mechanism is important at lower q, our analysis will have to be redone with it properly included. Nevertheless, the general improvement obtained for the (e,e'), (p,p'), (p,n), and (γ,π^+) reactions when the new wave functions are used suggests that they may be the most reliable phenomenological wave functions obtained to date.

ACKNOWLEDGMENTS

We would like to thank our colleagues at the University of Massachusetts, Dr. G. A. Peterson, Dr. P. J. Ryan, and Dr. B. Parker, for their assistance in the data acquisition. We are also grateful to Dr. L. Tiator for providing us with the calculations presented in Fig. 9 and Dr. L. E. Wright for further discussions of the (γ,π^+) process. This work was supported by the U.S. Department of Energy under Contract No. DE-AC02-76ER02853.

*Present address: Department of Physics, Wittenberg University, Springfield, OH 45501.

†Present address: Los Alamos National Laboratory, Los Alamos, NM 87545.

[1]D. R. Inglis, Rev. Mod. Phys. **25**, 390 (1953).

[2]B. Jancovici and I. Talmi, Phys. Rev. **95**, 289 (1954).

[3]R. Sherr, J. B. Gerhart, H. Horie, and W. F. Hornyak, Phys. Rev. **100**, 445 (1955).

[4]J. P. Elliot, Philos. Mag. **1**, 503 (1956).

[5]W. M. Visscher and R. A. Ferrell, Phys. Rev. **107**, 781 (1957).

[6]E. Baranger and S. Meshkov, Phys. Rev. Lett. **1**, 30 (1958).

[7]H. A. Weidenmuller, Nucl. Phys. **36**, 151 (1962).

[8]W. W. True, Phys. Rev. **130**, 1530 (1963).

[9]L. Zamick, Phys. Lett. **21**, 194 (1966).

[10]H. J. Rose, O. Hauser, and E. K. Warburton, Rev. Mod. Phys. **40**, 591 (1968).

[11]N. Ensslin, Ph.D. dissertation, Massachusetts Institute of Technology, 1972 (unpublished).

[12]N. Ensslin, W. Bertozzi, S. Kowalski, C. P. Sargent, W. Turchinetz, C. F. Williamson, S. Fivozinsky, J. Lightbody, and S. Penner, Phys. Rev. C **9**, 1704 (1974).

[13]H. W. Baer, J. A. Bistirlich, N. de Botton, S. Cooper, K. M. Crowe, P. Truol, and J. D. Vergados, Phys. Rev. C **12**, 921 (1975).

[14]S. Cohen and D. Kurath, Nucl. Phys. **73**, 1 (1965).

[15]R. L. Huffman, R. S. Hicks, J. Dubach, B. Parker, M. A. Plum, G. Lahm, R. Neuhausen, and J. C. Bergstrom, Phys. Lett. **139B**, 249 (1984).

[16]N. Ensslin, L. W. Fagg, R. A. Lindgren, W. L. Bendel, and E. C. Jones, Jr., Phys. Rev. C **19**, 569 (1979).

[17]G. Lahm, Ph.D. dissertation, University of Mainz, 1982 (unpublished).

[18]B. Goulard, B. Lorazo, H. Primakoff, and J. D. Vergados, Phys. Rev. C **16**, 1999 (1977).

[19]B. Lorazo and B. Goulard, Can. J. Phys. **58**, 388 (1980).

[20]K. Matsuda, Y. Nagahara, Y. Oda, M. Takeda, N. Takana, T. Yamazaki, and C. Hu, J. Phys. Soc. Jpn. **15**, 760 (1960).

[21]G. M. Crawley, S. M. Austin, W. Benenson, V. A. Madsen, F. A. Schmittroth, and M. J. Stomp, Phys. Lett. **32B**, 92 (1970).

[22]T. H. Curtis, H. F. Lutz, D. W. Heikkinen, and W. Bartolini, Nucl. Phys. **A165**, 19 (1971).

[23]C. W. Rogers, P. Fessenden, and V. A. Madsen, Bull. Am. Phys. Soc. **16**, 830 (1971).

[24]H. F. Lutz, D. W. Heikkinen, and W. Bartolini, Nucl. Phys. **A198**, 257 (1972).

[25]L. F. Hansen, S. M. Grimes, J. L. Kammerdiener, and V. A. Madsen, Phys. Rev. C **8**, 2072 (1973).

[26]J. R. Comfort, Sam M. Austin, P. T. Debevec, G. A. Moake, R. W. Finlay, and W. G. Love, Phys. Rev. C **21**, 2147 (1980).

[27]S. H. Fox and S. M. Austin, Phys. Rev. C **21**, 1133 (1980).

[28]W. D. Cornelius, J. M. Moss, and T. Yamaya, Phys. Rev. C **23**, 1364 (1981).

[29]Y. Aoki, S. Kunori, K. Nagano, Y. Toba, and K. Yagi, Nucl. Phys. **A382**, 269 (1982).

[30]T. N. Taddeucci, J. Rapaport, C. C. Foster, and J. R. Comfort, Phys. Rev. C **28**, 969 (1983).

[31]T. N. Taddeucci, R. R. Doering, A. Galonsky, and S. M. Austin, Phys. Rev. C **29**, 764 (1984).

[32]R. R. Doering, T. N. Taddeucci, A. Galonsky, and D. M. Patterson, Phys. Rev. C **20**, 1627 (1979).

[33]C. Wong, J. D. Anderson, V. A. Madsen, F. A. Schmittroth, and M. J. Stomp, Phys. Rev. C **3**, 1904 (1971).

[34]C. Wong, J. D. Anderson, J. McClure, B. Pohl, V. A. Madsen, and F. A. Schmittroth, Phys. Rev. **160**, 769 (1967).
[35]K. Rohrich, L. Tiator, G. Kobshall, Ch. Reifferscheid, Ch. Schmitt, V. H. Walther, K. Weinand, and L. E. Wright, Phys. Lett. **153B**, 203 (1985).
[36]B. H. Cottman, K. Min, P. Stoler, P. K. Teng, E. J. Winhold, M. Yamazaki, P. F. Yergin, A. M. Bernstein, K. I. Blomqvist, J. H. J. Distelbrink, J. A. Nelson, K. Rohrich, C. Schmitt, L. Tiator, V. H. Walther, G. Audit, S. A. Dytman, and L. E. Wright, Phys. Rev. Lett. **55**, 684 (1985).
[37]C. A. Levinson and M. K. Banerjee, Ann. Phys. (N.Y.) **2**, 471 (1957).
[38]W. Bertozzi, M. V. Hynes, C. P. Sargent, C. Creswell, P. C. Dunn, A. Hirsch, M. Leitch, B. Norum, F. N. Rad, and T. Sasanuma, Nucl. Instrum. Methods **141**, 457 (1977).
[39]W. Bertozzi, M. V. Hynes, C. P. Sargent, W. Turchinetz, and C. Williamson, Nucl. Instrum. Methods **162**, 211 (1979).
[40]G. A. Peterson, J. B. Flanz, D. V. Webb, H. deVries, and C. F. Williamson, Nucl. Instrum. Methods **160**, 375 (1970).
[41]B. L. Parker, Ph.D. dissertation, University of Massachusetts, 1985 (unpublished).
[42]F. Borkowski, P. Peuser, G. G. Simon, V. H. Walther, and R. D. Wendling, Nucl. Phys. **A222**, 269 (1974).
[43]R. P. Singhal, J. Dubach, R. S. Hicks, R. A. Lindgren, B. Parker, and G. A. Peterson, Phys. Rev. C **28**, 513 (1983).
[44]R. S. Hicks, A. Hotta, J. B. Flanz, and H. deVries, Phys. Rev. C **21**, 2177 (1980).
[45]J. R. Moreira, R. P. Singhal, and H. S. Caplan, Can. J. Phys. **49**, 1434 (1971).
[46]F. Ajzenberg-Selove, Nucl. Phys. **A360**, 1 (1981).
[47]R. S. Willey, Nucl. Phys. **40**, 529 (1963).
[48]T. W. Donnelly and W. C. Haxton, At. Data Nucl. Data Tables **23**, 103 (1979).
[49]T. deForest and J. D. Walecka, Adv. Phys. **15**, 1 (1966).
[50]R. Simon, Ph.D. dissertation, University of Mainz, 1978 (unpublished).
[51]J. C. Bergstrom, U. Deutschmann, and R. Neuhausen, Nucl. Phys. **A327**, 439 (1979).
[52]J. B. Flanz, R. S. Hicks, R. A. Lindgren, G. A. Peterson, J. Dubach, and W. C. Haxton, Phys. Rev. Lett. **43**, 1922 (1979).
[53]R. S. Hicks, J. Dubach, R. A. Lindgren, B. Parker, and G. A. Peterson, Phys. Rev. C **26**, 339 (1982).
[54]R. S. Hicks, R. L. Huffman, R. A. Lindgren, G. A. Peterson, M. A. Plum, and J. Button-Shafer (unpublished).
[55]R. L. Huffman, Ph.D. dissertation, University of Massachusetts, 1985 (unpublished).
[56]R. Schaeffer and J. Raynal, distorted wave proton scattering computer code DWBA70, 1970 (unpublished).
[57]G. Bertsch, J. Borysowicz, H. McManus, and W. G. Love, Nucl. Phys. **A284**, 399 (1977).
[58]W. G. Love, in *Proceedings of the Telluride Conference on the (p,n) Reaction and the Nucleon-Nucleon Force, Telluride, Colorado, 1979*, edited by C. D. Goodman *et al.* (Plenum, New York, 1980), p. 23.
[59]W. G. Love and M. A. Franey, Phys. Rev. C **31**, 488 (1985).
[60]B. C. Clark, S. Hama, R. L. Mercer, L. Ray, and B. D. Serot, Phys. Rev. Lett. **50**, 1644 (1983).
[61]J. A. McNeil, J. R. Shepard, and S. J. Wallace, Phys. Rev. Lett. **50**, 1439 (1983).
[62]J. R. Shepard, J. A. McNeil, and S. J. Wallace, Phys. Rev. Lett. **50**, 1443 (1983).
[63]J. R. Comfort and B. C. Karp, Phys. Rev. C **21**, 2162 (1977).
[64]L. Tiator, private communication.
[65]K. Rohrich *et al.*, private communication.
[66]P. K. Teng, B. H. Cottman, L. Ghedira, K. Min, P. Stoler, E. J. Winhold, M. Yamazaki, P. F. Yergin, A. M. Bernstein, K. I. Blomqvist, J. H. J. Distelbrink, J. A. Nelson, K. Rohrich, Ch. Schmitt, L. Tiator, V. H. Walther, S. A. Dytman, and L. E. Wright, Phys. Lett. **177B**, 25 (1986).